

A&A manuscript no.
(will be inserted by hand later)

Your thesaurus codes are:
03(11.01.01; 11.09.4; 11.13.1; 11.16.1)

ASTRONOMY
AND
ASTROPHYSICS

Reddenings and metallicities in the LMC and SMC from Strömgren CCD photometry [★] ^{★★}

S.S. Larsen,^{1,2} J.V. Clausen¹, and J. Storm³

¹ Niels Bohr Institute for Astronomy, Physics and Geophysics, Astronomical Observatory, Juliane Maries Vej 30, DK-2100 Copenhagen Ø, Denmark

email: jvc@astro.ku.dk

² UC Observatories / Lick Observatory, University of California, Santa Cruz, CA 95064, USA

email: soeren@ucolick.org

³ Astrophysikalisches Institut Potsdam, An der Sternwarte 16, D-14482 Potsdam, Germany

email: jstorm@aip.de

Received 25 May 2000 / Accepted 11 October 2000

Abstract. The *individual* reddenings for B stars in two fields in the Small Magellanic Cloud (SMC) and two fields in the Large Magellanic Cloud (LMC) are determined by means of Strömgren *uvby* CCD photometry. In both LMC fields we find a foreground reddening of $E(B - V) = 0.085 \pm 0.02$, and for the SMC fields we find $E(B - V) = 0.070 \pm 0.02$. In addition to the foreground reddening we find contributions from reddening intrinsically in the Clouds up to $E(B - V) \sim 0.21$. The intrinsic contribution is not correlated with position within our $\sim 6' \times 4'5$ CCD fields but varies in an essentially random way. Unless the reddening is measured for a particular object, it will be uncertain by ± 0.035 (best case, far from the central bars) to more than ± 0.10 (close to the central bars).

The Strömgren *vby* photometry has been used to derive metallicities for GK giant stars in the observed fields. Adopting average reddenings we obtain mean metallicities which are consistent with those found from spectroscopic studies of F and G supergiants (Westerlund 1997), but with a considerable scatter in the derived metallicities, from $[\text{Fe}/\text{H}] \approx -2.0$ to $[\text{Fe}/\text{H}] \gtrsim 0$. A significant fraction of the scatter is, however, due to reddening variations rather than being intrinsic. The possible existence of high metallicity stars should be investigated further using spectroscopic methods.

Key words: Magellanic Clouds – abundances – ISM – photometry

1. Introduction

This paper describes an investigation of reddenings and metallicities in two fields in each of the Magellanic Clouds by means of Strömgren CCD photometry. For the first time, the reddening variations on very small scales (~ 1 pc, limited by the surface density of B stars) have been examined from Strömgren photometry. A detailed analysis of the metallicities of GK giant stars is performed, with special emphasis on the problems that arise from an incomplete knowledge of the individual reddenings of the stars. The metallicities derived for GK giants from Strömgren photometry are very sensitive to the assumed reddening, but because we have an estimate of the scatter in the reddening distributions from the early-type stars we are able to give quantitative estimates of the uncertainty on metallicities for individual GK giants.

The disagreement in the literature on the reddening for Magellanic Cloud stars has been remarkably large. Part of the controversy probably arises from an insufficient distinction between foreground reddening and reddening intrinsically in the Clouds. Grieve & Madore (1986) found that some stars in the SMC have reddenings as high as $E(B - V) = 0.20$ with an average of around $E(B - V) = 0.09$, while the maximum for the LMC is $E(B - V) = 0.3$ and the average is $E(B - V) = 0.1$. Grieve & Madore (1986) also noted that in the LMC the stars with high reddenings are predominantly concentrated in the neighbourhood of the 30 Doradus complex. In a review paper, Bessel (1991) concluded that while it has been claimed that the reddening is as low as $E(B - V) = 0.01$ or 0.02 for both Clouds, several investigations arrive at considerably higher reddenings, up to $E(B - V) = 0.1$ or even more. From studies of a (fairly small) section of the LMC, Harris et al. (1997) determined a mean total $E(B - V)$ of 0.20 with a non-Gaussian tail to high values. Oestreicher et al. (1995) and Oestreicher & Schmidt-

Send offprint requests to: S.S. Larsen

[★] Based on observations carried out with the Strömgren Automatic Telescope (SAT) and the Danish 1.54 meter telescope at ESO, La Silla

^{★★} The CCD *uvby* photometry is available in electronic form at the CDS via anonymous ftp to 130.79.128.5 or via <http://cdsweb.u-strasbg.fr/Abstract.html>

Kaler (1996) determined foreground reddenings and intrinsic reddenings for the LMC, and found that the foreground reddening generally varies from $E(B - V) = 0.0$ to $E(B - V) = 0.1$ across the face of the LMC, while reddenings up to $E(B - V) = 0.8$ were seen for some of the brightest A and B supergiants. However, the extreme reddenings were interpreted as being caused by circumstellar dust shells, an assumption which was supported by the fact that for the fainter stars only more modest reddenings, up to $E(B - V) = 0.20$, were detected. Schlegel et al. (1998) report typical foreground reddenings of $E(B - V) = 0.075$ (LMC) and 0.037 (SMC), respectively. Using $UBVI$ photometry, Zaritsky (1999) also found a dependence of reddening on spectral type, with stars hotter than ~ 12000 K having visual extinctions up to several tenths of a magnitude larger than cooler stars. Recently, Romaniello et al. (2000) found a mean $E(B - V)$ of 0.20 mag around SN 1987A with a scatter of 0.072 mag, claimed to be at least twice the measurement errors.

Many investigations have aimed at deriving metallicities for different types of objects (HII regions, planetary nebulae, single stars) in the Magellanic Clouds. This is not the place to give an extensive review of all of them; we refer to Westerlund (1990, 1997). A general picture of a roughly exponential increase in metal abundance with time over the last 10 Gyr is often quoted for both galaxies. From studies of the surroundings of six LMC clusters, Dirsch et al. (2000) have determined an age-metallicity relation which shows a strong increase in the metallicity starting around 2–3 Gyrs ago. For very young objects mean $[\text{Fe}/\text{H}]$ values are about -0.2 (LMC) and -0.5 (SMC), respectively, whereas “canonical” field star metallicities of around $[\text{Fe}/\text{H}] = -0.3$ for the LMC and $[\text{Fe}/\text{H}] = -0.65$ for the SMC are often used.

The Strömgren $uvby\beta$ photometric system was originally designed for the study of BAF stars (Strömgren 1966). It has, however, turned out to be very useful also for investigations of other types of stars. Bond (1980) demonstrated that metallicities can be derived for red giants by means of the Strömgren $(b - y)_0$ and m_0 indices. In nearby galaxies, such as the Magellanic Clouds, the Strömgren system thereby provides us with a potentially very powerful tool for studying the metallicities of large numbers of red field giant stars.

Several *spectroscopic* studies of cool supergiants reach the canonical metallicities and a scatter of about ± 0.2 dex (e.g. Spite & Spite 1987; Olszewski et al. 1991; Hill 1999), whereas attempts to derive metallicities for red field giants from Strömgren photometry (Hilker et al. 1995 (HRG95); Grebel & Richtler 1992 (GR92); Dirsch et al. 2000) have failed to reproduce them. GR92 studied the neighbourhood of the young cluster NGC 330 in the SMC and found $[\text{Fe}/\text{H}] = -1.26$ for the cluster itself, whereas the surrounding field stars had an average metallicity of $[\text{Fe}/\text{H}] = -0.74$ with a large spread. HRG95 found $[\text{Fe}/\text{H}] = -0.93 \pm 0.16$ for NGC 330 and metallicities in the range

Table 1. The observed fields. For comparison, the positions for the optical centers of the bars of SMC and LMC are included.

Field ID	$\alpha(2000.0)$	$\delta(2000.0)$
LMC	$05^{\text{h}}24^{\text{m}}$	$-69^{\circ}44'$
HV982	$05^{\text{h}}29^{\text{m}}53^{\text{s}}$	$-69^{\circ}09'23''$
HV12578	$05^{\text{h}}21^{\text{m}}32^{\text{s}}$	$-66^{\circ}21'15''$
SMC	$00^{\text{h}}53^{\text{m}}$	$-72^{\circ}49'$
HV1433	$00^{\text{h}}47^{\text{m}}11^{\text{s}}$	$-73^{\circ}41'18''$
HV11284	$00^{\text{h}}49^{\text{m}}43^{\text{s}}$	$-72^{\circ}51'10''$

$[\text{Fe}/\text{H}] = -2.0$ to -0.2 for the field stars, with a peak at $[\text{Fe}/\text{H}] \sim -1.0$. For the red giants in the LMC cluster NGC 1866, HRG95 found a metallicity of $[\text{Fe}/\text{H}] = -0.43 \pm 0.18$, while the field stars also here showed a large variation in metallicity with a peak at $[\text{Fe}/\text{H}] = -0.7$. Dirsch et al. (2000) generally find metallicities lower than -0.3 for six relatively young LMC clusters and their surrounding fields.

In this paper we first derive reddenings for early-type stars in each of the four fields using new CCD Strömgren photometry. Metallicities are then derived for red giant stars in the same four fields, also using Strömgren photometry. The uncertainties on the derived metallicities are then discussed, with particular emphasis on the scatter resulting from an inaccurate knowledge of the reddenings of individual red giant stars.

2. Observations and reductions

The observations were carried out during several observing runs in 1992 – 1995 with the Danish 1.54 m telescope at ESO, La Silla, equipped with a direct camera and CCD #28 (a 1024×1024 Tek device). This combination of telescope and CCD yields a field size of about $6'.5 \times 6'.5$, although the effective field size was somewhat smaller, typically $6' \times 4'.5$, because we combined each image from many individual frames that were not perfectly aligned. The image scale is $0''.38$ / pixel. Four fields centered on eclipsing variable stars were observed, two in the SMC and two in the LMC (Table 1). The HV12578 field is located close to the region E of the *ESO Key Programme on Coordinated Investigations of Selected Regions in the Magellanic Clouds* (de Boer et al. 1989) in the northern part of the LMC, whereas the HV982 field is located close to the Key Programme region F, in the northern outskirts of the LMC Bar, close to the 30 Doradus complex. The HV1433 and HV11284 fields are located on each side of the Key Programme B region, in the southern part of the SMC.

The observations were originally obtained for a study of eclipsing binary B stars (Clausen et al., in prep.). Therefore, the data set consists of a large number of short individual exposures (typically 5 minutes in vby and 20 min-

Table 2. Data for the combined frames. The first two columns are self-explanatory, the third column gives the number of frames used in the combined frames, the total integration time (in minutes) is listed in the fourth column, and the last column gives the resulting seeing measured on the combined frames.

Field	filter	N	T_{exp}	seeing
HV982	u	67	640	1''.5
	v	87	250	1''.3
	b	62	180	1''.4
	y	199	500	1''.3
HV12578	u	28	560	1''.5
	v	40	200	1''.4
	b	28	140	1''.4
	y	100	500	1''.3
HV1433	u	16	290	1''.6
	v	24	160	1''.4
	b	21	140	1''.4
	y	53	272	1''.4
HV11284	u	21	420	1''.5
	v	29	145	1''.4
	b	31	155	1''.4
	y	84	420	1''.4

utes in u). Initial reductions, essentially flatfielding and bias subtraction, were carried out using standard IRAF¹ tools. For each field and each filter, exposures with seeing better than 1''.7 and with sky background levels lower than a certain threshold were selected, and these exposures were then summed using the IRAF task **imcombine**. Hence, equivalent integration times of typically 3–5 hours in y , b and v , and 5–10 hours in u were obtained (see Table 2). The combination of many short exposures offered the advantage that cosmic ray events could be effectively eliminated, using the **crreject** option in **imcombine**.

The calibration to the standard $uvby$ system was based on observations of secondary standard stars defined by photoelectric observations with the Strömgren Automatic Telescope (SAT) at ESO, La Silla (see Clausen et al. 1997). The SAT observations were carried out simultaneously with the 1.54 m observations, and also provided extinction coefficients for the calibration of the CCD photometry. The rms difference between the transformed CCD magnitudes and SAT magnitudes of the secondary standard stars was less than 0.01 in $(b - y)$ and around 0.015 in c_1 . Although the individual CCD exposures were obtained during several observing runs, the instrumental system was stable enough that we did not find any reason to use separate transformations for the different runs, except for zero-point differences. This indicates that the properties of the filters and the CCD are quite stable, while the

zero-point differences may be due to changes in the reflectivity of telescope mirrors, gain settings for the CCD camera electronics etc.

For the CCD photometry we used DAOPHOT II (Stetson 1987) running within IRAF. The internal accuracy of the CCD photometry was typically around 0.01 mag in $(b - y)$ and 0.03 mag in c_1 and m_1 for stars brighter than $V \sim 19$, while we find that systematic errors due to the determination of zero-points for the PSF photometry relative to the aperture photometry of the standard stars are on the order of 0.01 mag in all filters.

It is a notorious problem to get the zero-points of the crowded-field PSF photometry relative to the standard aperture photometry right, in particular in a case like ours where there are no bright, isolated stars present in the fields. We approached the problem as follows: First, a set of individual exposures in the four Strömgren filters were selected for each field. Photometry was obtained on all stars in the selected frames following the usual DAOPHOT procedure, and then all stars except for a few bright ones were subtracted using the task **substar** in the DAOPHOT package. The few stars that were not subtracted were then measured using standard aperture photometry, thus providing a set of possible “tertiary standard stars” in each frame. The final tertiary standard stars were selected from careful curves of growth analyses; see Larsen (1996) for further details. The PSF photometry of the combined frames was then tied into the aperture photometry system using the tertiary standards in each frame.

Finally Be stars were identified from $H\alpha$ exposures and only between 5 and 39 of these stars were found in the various fields. It was also tested that foreground stars cause no serious problems; see Larsen (1996) for details.

3. Reddenings

3.1. Reddenings from Strömgren photometry

The classical way to derive reddening from Strömgren photometry is to use the β index and $(b - y)$ which are very well correlated for F-type stars (Crawford 1975). The β index is unaffected by reddening, so the reddening can be determined by comparing the observed $(b - y)$ to the value expected from the standard β - $(b - y)$ relation. However, in the Magellanic Clouds the F-type main sequence stars are much too faint to be reached by our photometry, and there are additional problems with the β photometry and its calibration because of the non-vanishing radial velocities of the clouds (Knude 1993).

However, the Strömgren system also provides a way to determine reddening for the more luminous early-type stars (A0 and earlier, Strömgren 1966). Instead of $(b - y)$ and β , the reddening for early-type stars is derived from the $(b - y)$ and c_1 indices, following the “standard iterative procedure” described e.g. by Crawford et al. (1970).

¹ IRAF is distributed by the National Optical Astronomical Observatories, which are operated by the Association of Universities for Research in Astronomy, Inc. under contract with the National Science Foundation.

Both $(b - y)$ and c_1 are temperature indicators for stars of spectral type earlier than A0, and for such stars the de-reddened indices $(b - y)_0$ and c_0 are related to each other through a standard relation in much the same way as are $(b - y)$ and β in the case of F stars. The calibration of the $(b - y)_0 - c_0$ standard relation was empirically established by Crawford (1978), and agrees well with Strömgen indices based on model atmosphere calculations for early-type stars (Grebel, private communication. See also Sec. 3.3 and Fig. 5). The basic assumption is then that any observed deviation from the standard relation is caused by reddening.

The reddening vector in the $(b - y), c_1$ diagram is nearly horizontal so the reddening of a star can, to the first order, be estimated simply as the difference between the observed $(b - y)$ and the intrinsic value $(b - y)_0$ corresponding to the observed c_1 according to the standard relation:

$$E(b - y) \approx (b - y) - (b - y)_0(c_1)$$

With this initial estimate of the reddening, the c_1 index can be corrected and a new reddening can be derived. Usually only one or two iterations are required.

Due to the smaller wavelength difference between the b and y filters compared to the Johnson B and V filters, $E(B - V)$ is somewhat larger than $E(b - y)$, as can be shown from the standard law for interstellar extinction (Savage & Mathis 1979). More specifically, $E(B - V)$ and $E(b - y)$ are related through the following expression:

$$E(B - V) = 1.4 \times E(b - y) \quad (1)$$

A very convenient point regarding the de-reddening of stars earlier than spectral type A0 is that the β index is not required. However, because the c_1 index involves the u filter ($c_1 = (u - v) - (v - b)$), it has until recently been a time-consuming process to acquire sufficiently deep photometry for stars in the Magellanic Clouds with available CCD detectors.

3.2. Selection of B stars

In principle, the selection of early-type stars is most effectively carried out in the Strömgen system using the two reddening free indices

$$[m_1] = m_1 + 0.30(b - y)$$

and

$$[c_1] = c_1 - 0.20(b - y)$$

According to Strömgen (1966) and Olsen (1979) the $[m_1], [c_1]$ diagram should resemble the one in Fig. 1. The early-type stars are located in the left part of the diagram, on the part where $[c_1]$ is increasing as a function of $[m_1]$. The lower, right border of the band containing the early-type stars is defined quite well by a straight line given by the equation

$$[c_1] = 12 \times [m_1] - 0.88 \quad (2)$$

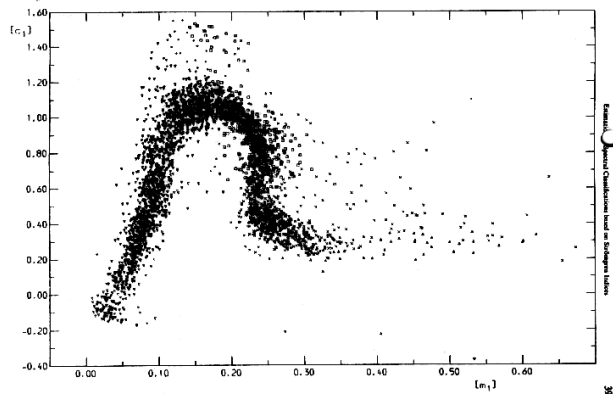


Fig. 1. $[m_1], [c_1]$ diagram of bright galactic stars (Olsen, 1979)

(E. H. Olsen, private communication). The exact location of the line is only critical for $[c_1] > 0.9$, since no stars are found immediately to the right of it for lower $[c_1]$ values.

The $[m_1], [c_1]$ diagrams for stars in the LMC/SMC fields with $\text{err}(c_1) < 0.10$ mag (corresponding to $V \lesssim 19.5$) are shown in Fig. 2. Obviously, they are not quite similar to the diagram shown in Fig. 1. The line separating early-type stars and stars of later types passes right through the distribution of points even for low $[c_1]$ values, and many stars are located inside the supposedly empty “loop”.

We have made several attempts at understanding this effect. The observations and data reduction procedures have been carefully checked to ensure that the effect is not a manifestation of some error in the stacking procedure, the cosmic ray elimination process or the use of DAOPHOT. This has been done by using the PSF fitting programme DoPHOT (Schechter et al. 1993) on a set of single $uvby$ frames without removal of cosmic rays. Apart from the expected larger scatter, the diagrams look qualitatively identical to the ones based on the full data set.

Could the peculiar $[m_1], [c_1]$ diagrams result from the lower metallicities in the Magellanic Clouds relative to local stars from which Fig. 1 was derived? In order to test this we obtained theoretical $[m_1], [c_1]$ colours for a set of stellar isochrones from the Padua group (Girardi et al. 2000), transformed into Strömgen colours using 1997 versions of Kurucz model atmospheres (Kurucz 1979, 1992). In Fig. 3 we show synthetic $[m_1], [c_1]$ diagrams for four different metallicities ($[\text{Fe}/\text{H}] = 0, -0.3, -0.6$ and -2.0). Each panel contains 5 isochrones corresponding to ages between 10^7 and 10^9 years. Only stars in the magnitude interval $-1 < M_V < -4$, roughly corresponding to the range covered by our data, have been included in the plot. Gaussian distributed random errors of $\sigma = 0.05$ mag, about similar to the typical errors in the observations, have been added to each axis (note that the 0.10 mag error limit in c_1 is an *upper* limit). The plots in Fig. 3 do suggest a significant change in the appearance of the $[m_1], [c_1]$ diagrams for progressively lower metallicities in

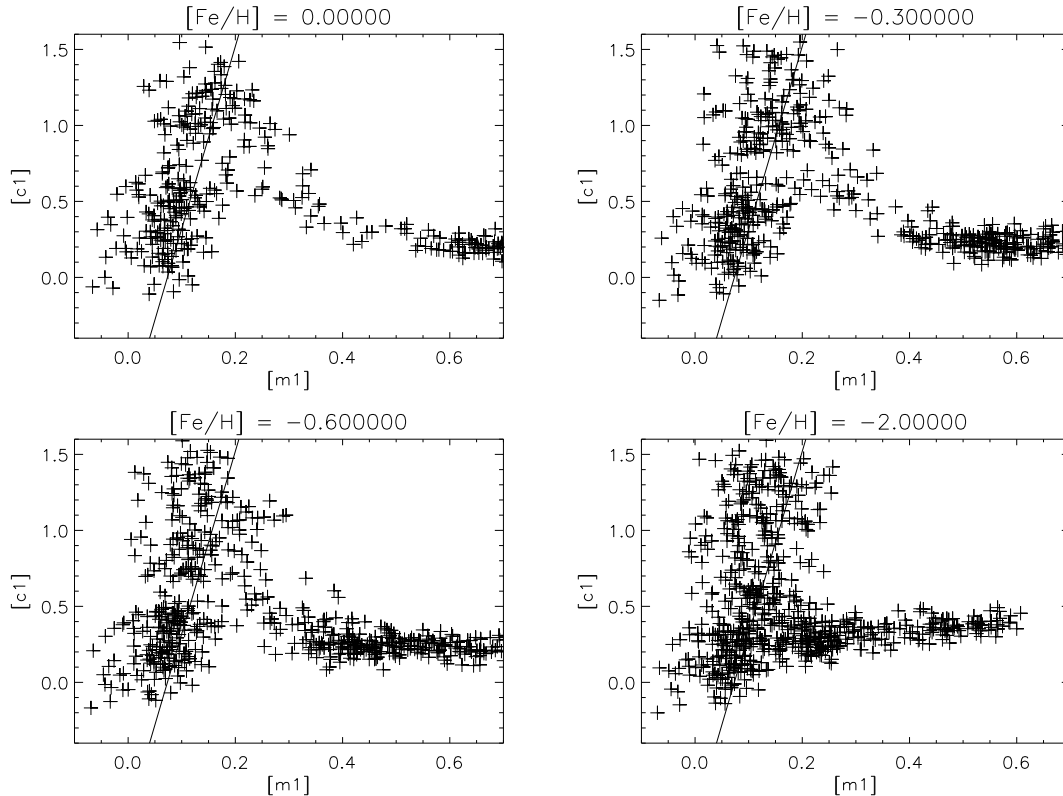


Fig. 3. Synthetic $[m_1], [c_1]$ diagrams based on Padua stellar models and Kurucz model atmospheres. Gaussian distributed random errors ($\sigma = 0.05$ mag) have been added to the synthetic $[m_1]$ and $[c_1]$ values.

the sense that more late-type stars will move in from the right and fill the empty region of the diagram. This effect is enhanced by the photometric scatter, although the early-type stars show only a very small systematic shift and for the HV982 field in particular, the theoretical $[m_1], [c_1]$ diagrams still do not provide a quite satisfactory match to the observations. Compared to Fig. 1, Fig. 2 shows only few early-type stars *above* the expected location, whereas random photometric errors in Fig. 3 cause equal amounts of stars to scatter upwards and downwards. However, the number of data points in different parts of the $[m_1], [c_1]$ diagram depends on the age distribution of the stars and unless this is taken into account, an exact match between the observed and simulated distributions cannot be expected.

We thus conclude that much of the apparently peculiar morphology of the observed $[m_1], [c_1]$ diagrams in the LMC and SMC could be due to a combination of lower metallicities and photometric errors. In any case, for our purpose the $[m_1], [c_1]$ diagram clearly is not a practical tool for selecting B stars.

Therefore, we have eventually chosen the alternative approach of selecting B stars directly as stars brighter than $V=19.0$ in the LMC and $V=19.4$ in the SMC and bluer than $(b-y) = 0.2$. The numbers of B stars in each field selected in this way range between 102 (for the HV12578

field) and 322 (for the HV982 field). The $(b-y)$ limit was chosen so that no confusion with red giants occurred, while nearly all main sequence stars would be included. The magnitude limit corresponds to $M_V \sim 0$. A potential problem is that evolved stars of later types than A0 could enter our sample, but these would have relatively high c_1 values, and any significant contamination by stars later than type A0 should therefore be visible in the $(b-y), c_1$ diagram as an excess of stars with $c_1 \approx 1$. No such excess is observed.

3.3. Foreground reddening

The $(b-y), c_1$ diagrams for B stars in each of the four fields are shown in Fig. 4 together with a line corresponding to the standard relation of Crawford (1978). The arrow shows the direction of the reddening vector. Only stars with a photometric error in $(b-y)$ of less than 0.015 and less than 0.05 in c_1 according to DAOPHOT were included in the analysis. Stars with a DAOPHOT χ estimate larger than 2 in *uvby* were also rejected regardless of the estimated error. The left-most boundary of the data points is quite well-defined, but offset with respect to the $(b-y)_0, c_0$ standard relation (due to foreground reddening), while the right-most boundary is more diffuse. In the SMC HV11284

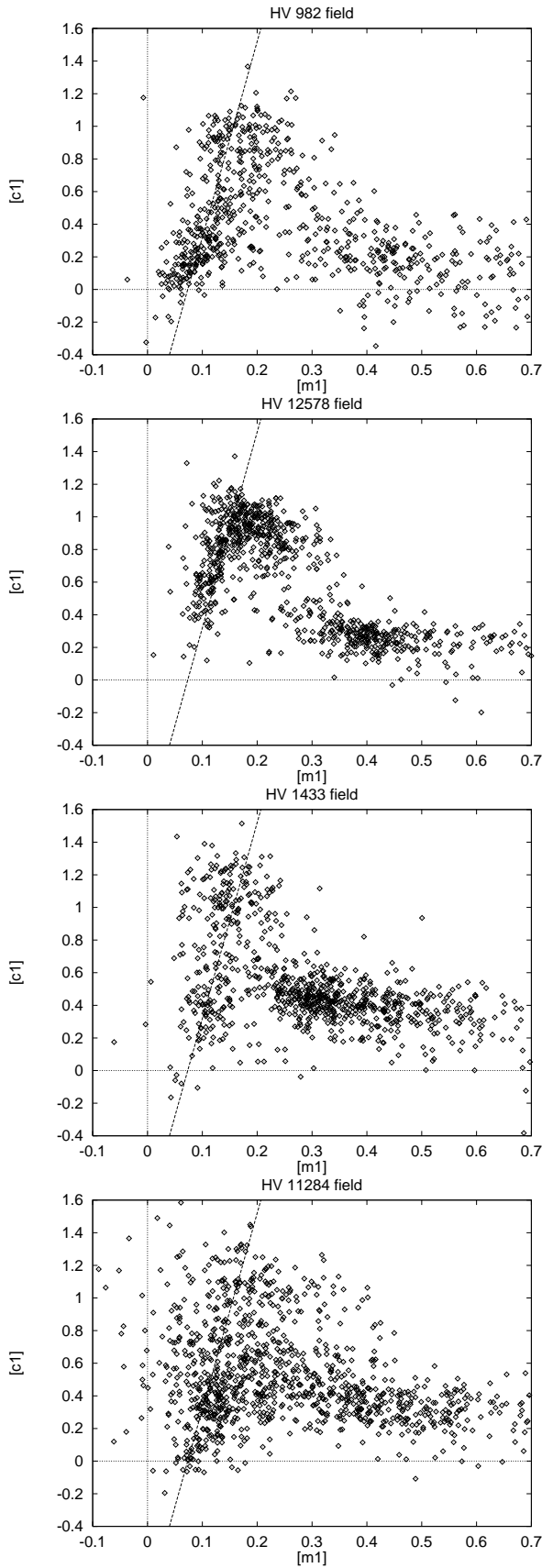


Fig. 2. $[m_1], [c_1]$ diagrams for the four LMC/SMC fields.

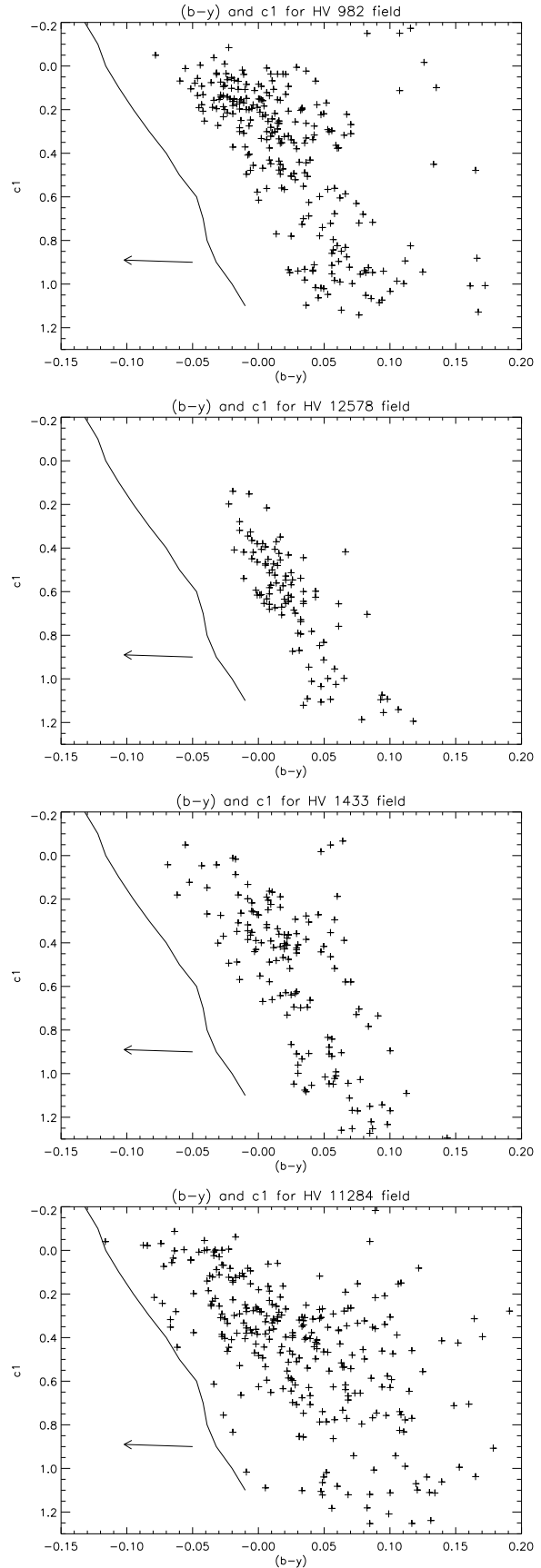


Fig. 4. $(b - y), c_1$ diagrams for B stars in the four fields. The arrow indicates the direction of the reddening vector.

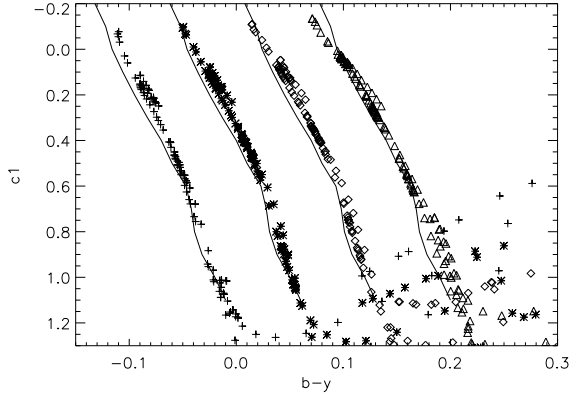


Fig. 5. Synthetic $b-y$, c_1 diagrams based on Padua stellar models and Kurucz model atmospheres. The plot shows data for four metallicities, offset by steps of 0.07 mag in $(b-y)$. Metallicities (left to right) are $[\text{Fe}/\text{H}] = 0, -0.3, -0.6$ and -2.0 .

Table 3. Basic reddening characteristics for the observed fields. Columns 2 and 3 give the minimum and average reddening for each field according to our investigation based on B stars.

Field	$E(b-y)$, min.	$E(b-y)$, avg.
LMC:		
HV982	0.060 ± 0.015	0.100
HV12578	0.060 ± 0.015	0.075
SMC:		
HV1433	0.050 ± 0.015	0.089
HV11284	0.050 ± 0.015	0.100

field we note the presence of a few stars with apparently very low reddenings.

Once again, we used the Padua isochrones combined with Kurucz atmospheres to test if the Crawford (1978) relation applies also to the metal-poorer LMC/SMC stars. The theoretical $(b-y)$, c_1 diagrams for stars with $1 < M_V < -4$ are shown in Fig. 5 for four different metallicities together with the Crawford relation. Like in Fig. 3, five different isochrones corresponding to ages between 10^7 and 10^9 years are included but no random errors are added in Fig. 5. The models and the empirical relation generally agree well for all metallicities and there are no evident trends with metallicity that would affect the reddening determinations, so we conclude that reddenings derived from the $(b-y)$, c_1 diagram are reliable.

The reddening distributions derived from the data in Fig. 4 as described in the previous section are shown in Fig. 6. The dashed Gaussians represent the average observational scatter. The lower limit of the reddening distribution is interpreted as being caused by Galactic foreground extinction. We estimate that this amounts to $E(b-y) = 0.060 \pm 0.015$ in both of the LMC fields and

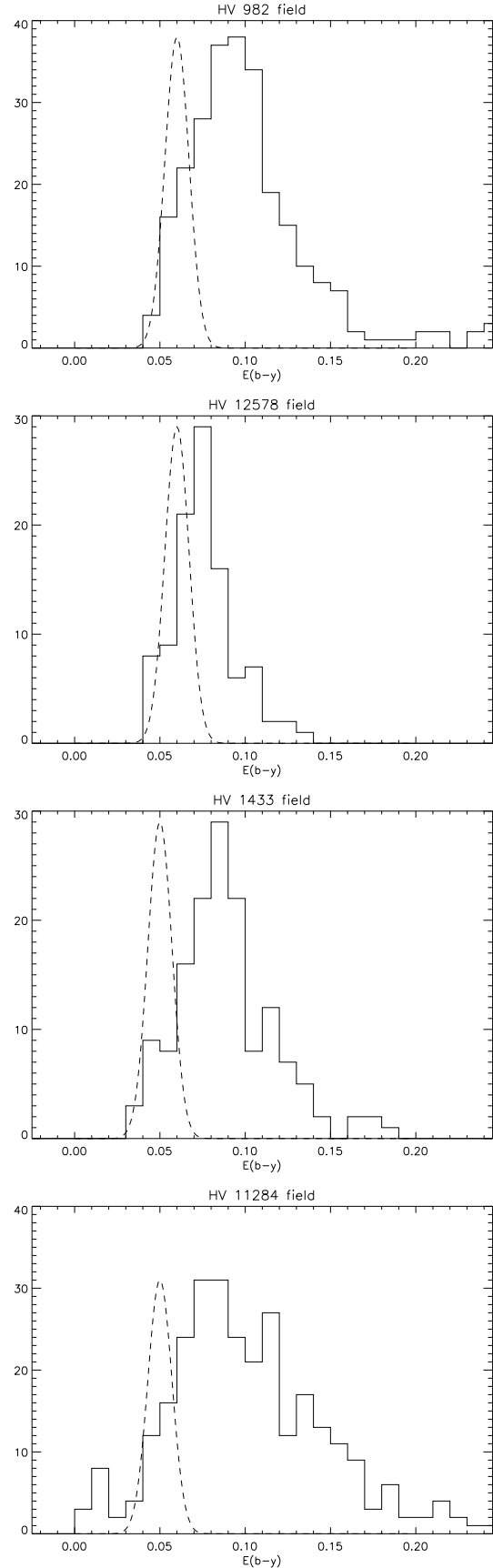


Fig. 6. Reddening histograms (B stars) for the four fields; see text for details.

$E(b - y) = 0.050 \pm 0.015$ in the SMC fields, corresponding to $E(B - V) = 0.085 \pm 0.02$ and $E(B - V) = 0.07 \pm 0.02$, respectively. The estimated errors in these reddenings are largely due to zero-point errors in the b and y photometry, while errors in c_1 do not affect the results significantly.

For the LMC fields, we can compare the foreground reddening determinations to the reddening map by Oestreicher et al. (1995), which predicts foreground reddenings of $E(B - V) = 0.045$ and $E(B - V) = 0.050$ in the HV12578 and HV982 fields. Thus, our estimated foreground reddenings are somewhat higher and agree well with the typical value of $E(B - V) = 0.075$ reported by Schlegel et al. (1998). However, their typical SMC value of $E(B - V) = 0.037$ is significantly lower than our results.

3.4. The correlation of reddening with position.

The width of the histograms representing the reddening distributions cannot be accounted for by observational uncertainties and must, consequently, represent real scatter in the reddenings of LMC/SMC B stars. This could either mean that the foreground reddening varies by as much as 0.1 in $E(B - V)$ within the fields, or that the B stars are subject to different amounts of reddening from the interstellar medium in the Clouds themselves, being located at different optical depths. In the first case, we would expect that reddenings are strongly correlated with the position in the image, whereas such a correlation would be weaker or absent if the variations are caused by depth effects. Of course, any intermediate scenario is in principle possible.

If reddening is correlated with position then the difference between the reddenings of two neighbouring stars will, on the average, be smaller than that of two widely separated stars. In order to investigate this effect, we used our measurements of individual B star reddenings to calculate the r.m.s. reddening difference between two stars as a function of their separation in the image. We denote the r.m.s. reddening difference between the reddening of a star and other stars at distances $[R \dots R + \Delta R[$ from it $C(R, \Delta R)$ where ΔR is the bin size. We found $\Delta R = 10$ pixels to be a reasonable bin size.

If reddening is correlated with position on scales smaller than some characteristic limit, $C(R, \Delta R)$ will decrease as R becomes smaller than the characteristic limit, which could for example depend on the typical size of interstellar clouds. ΔR is not a very critical parameter. It should be chosen sufficiently large that a reasonable number of stars will be located within an annulus of inner radius R and outer radius $R + \Delta R$. On the other hand, it should not be larger than the typical size of the structure we are looking for.

Figure 7 shows $C(R, \Delta R)$ for each field, with ΔR set to 10 pixels or roughly 4 arcseconds. There is no significant decrease in C even for quite small R , with a hint of such a decrease only in the SMC fields (HV1433, HV11284). At the same time, Fig. 7 also gives for each field an indication

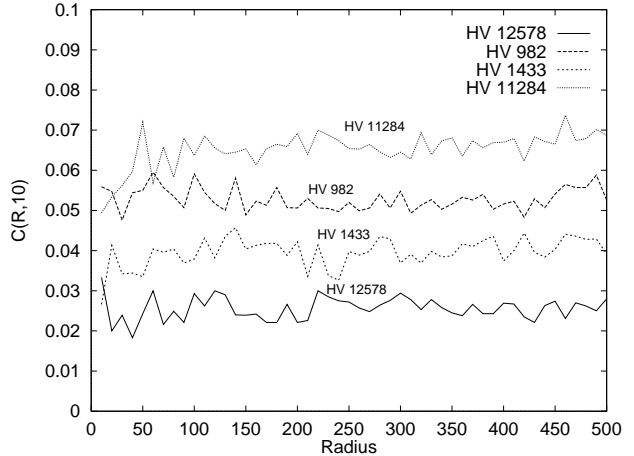


Fig. 7. The quantity $C(R, \Delta R)$, denoting the rms $E(b - y)$ difference between B stars located in the distance interval $[R \dots \Delta R[$ from each other. $R = 100$ (pixels) corresponds to $38''$.

of how large the typical error will be if just the average reddening of the field is used as an estimate of the reddening for a given star. This varies from one field to another, from $E(b - y) = 0.025$ in the HV12578 field to 0.07 in the HV11284 field, and it is clear that the error is in no case negligible. Based on the two fields we have observed in each galaxy, the contribution from internal reddening in the Clouds appears to decrease as a function of distance to the centre.

3.5. Discussion of reddenings

The previous section has shown a lack of correlation between reddening and position in the fields, even on the smallest scales on which this can be investigated by means of the present Strömgren photometry, i.e. a few arc seconds (for LMC and SMC, 1 pc corresponds to about $4''$ and $3''5$, respectively).

Many stars have reddenings much larger than the Galactic foreground contribution, in some fields up to $E(b - y) = 0.15$ ($E(B - V) = 0.21$) or so. Because the reddening is not correlated with the position in the field, we conclude that the variations are most likely due to the stars being located at different depths in the Magellanic Clouds. Therefore, the difference between the maximum and minimum reddening in each field presumably represents the total reddening when looking through the LMC or SMC at the corresponding position.

It is of interest to compare our results with the investigation by Oestreicher & Schmidt-Kaler (1996). Their reddening map shows a lack of stars with high reddenings in the neighbourhood of the HV12578 field, in agreement with our results, whereas a large number of stars with relatively high reddenings are found near the 30 Dor region, again in agreement with our results. Oestreicher &

Schmidt-Kaler (1996) did not study the Small Magellanic Cloud. Olsen (1999) only found strong differential reddening in one out of four LMC fields observed with the HST, centered on the cluster NGC 1916 near the centre of the LMC bar.

As we shall see in the following section, the fact that average reddenings are only accurate to within several hundredths of a magnitude is potentially a serious problem for photometric studies of stars where reddenings cannot be directly determined, such as metallicity studies of GK giants in the Strömgren system (Hilker et al. 1995; Grebel & Richtler 1992; Dirsch et al. 2000).

4. Metallicities

4.1. Metallicities for GK giants

For GK giants it is appropriate to define the metallicity calibration directly in terms of $(b - y)$ and m_1 instead of using the δm_1 notation for F dwarfs of e.g. Crawford (1975). We use the calibration by Hilker (2000),

$$[\text{Fe}/\text{H}] = \frac{m_0 + a_1(b - y)_0 + a_2}{a_4 + a_3(b - y)_0} \quad (3)$$

with $a_1 = -1.277 \pm 0.050$, $a_2 = 0.331 \pm 0.035$, $a_3 = 0.324 \pm 0.035$ and $a_4 = -0.032 \pm 0.025$, valid for $-2.0 < [\text{Fe}/\text{H}] < 0.0$. When plotted in the $(b - y)_0, m_0$ diagram (i.e. after de-reddening), GK giant stars of the same metallicity will fall along a straight line, independently of luminosity. Compared to an earlier calibration of $[\text{Fe}/\text{H}]$ as a function of $(b - y)_0$ and m_0 by Grebel & Richtler (1992), the Hilker (2000) calibration yields somewhat lower metallicities, especially at low metallicities. The difference amounts to about 0.1 dex for $[\text{Fe}/\text{H}] \sim -0.5$ and increases to ~ 0.25 dex for $[\text{Fe}/\text{H}] \sim -1.5$.

For a “typical” GK giant with $(b - y)_0 = 0.75$ and $m_0 = 0.5$, errors in v , b and y of 0.01 magnitudes correspond to a total error in the derived metallicity of about 0.16 dex, with the most significant contribution to the total error arising from the b band error. Similarly, an error in the estimated reddening $E(b - y)$ of 0.01 mag translates to about 0.05 dex in the derived $[\text{Fe}/\text{H}]$. Hence, the derived metallicities are quite sensitive to errors in the measurements as well as in the assumed reddenings, and great care must be taken to avoid systematic errors which may shift the observed metallicity distributions by significant amounts.

In this section we analyze the metallicity distributions derived for GK giants using the calibration given by Eq. (3). Following Hilker (2000) we have used the calibration for stars with $0.5 < (b - y) < 1.1$. Additional selection criteria based on DAOPHOT parameters were $\text{err}(m_1) < 0.02$ and $\chi(y, b, v) < 2.0$. This resulted in about 100 – 200 stars for metallicity analysis in each field (see Table 4).

Figure 8 shows the $(b - y)_0, m_0$ diagrams for the four fields and the derived metallicity distributions are in Figure 9 (solid lines). The average reddenings given in Table

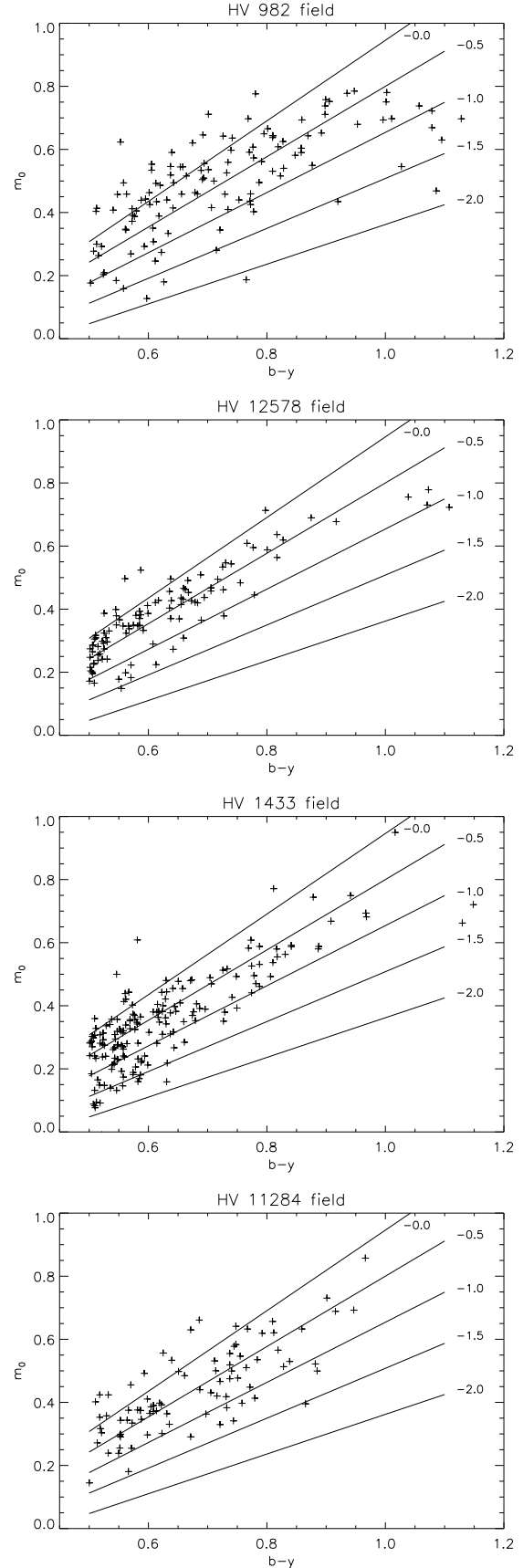


Fig. 8. $(b - y)_0, m_0$ diagrams for the four fields. The straight lines represent constant metallicities according to Eq. 3.

Table 4. Metallicity data for the four fields. Numbers in parantheses indicate the values when only stars with $[\text{Fe}/\text{H}] < 0.0$ are included. N is the number of GK giants used.

Field ID	N		[Fe/H](Mean)	[Fe/H](Med)	[Fe/H](Mode)
LMC:					
HV982	121	(92)	-0.40 (-0.65)	-0.32 (-0.54)	-0.15 (-0.33)
HV12578	102	(95)	-0.47 (-0.53)	-0.42 (-0.44)	-0.31 (-0.27)
SMC:					
HV1433	167	(155)	-0.68 (-0.76)	-0.64 (-0.66)	-0.56 (-0.46)
HV11284	86	(74)	-0.46 (-0.60)	-0.45 (-0.54)	-0.42 (-0.42)

3 have been used. Fig. 9 shows a significant scatter in the derived metallicities, from $[\text{Fe}/\text{H}] = -2.0$ up to around $[\text{Fe}/\text{H}] = 0$. In some of the fields the derived metallicity distributions include a number of stars with $[\text{Fe}/\text{H}] > 0$. However, as shown for the Milky Way globular cluster 47 Tuc by Dickens et al. (1979), stars with peculiar CNO abundances can mimic stars with a generally high metallicity. The effect of CN anomaly on metallicities derived from Strömgen photometry has also been illustrated by Richter et al. (1999). Furthermore, the $(b-y)_0, m_0$ metallicity calibration is valid only for subsolar metallicities. We therefore can not conclude with certainty from our data that stars with truly high metallicities exist in the LMC or SMC, while the possibility remains open. Spectroscopic studies will be needed in order to answer this question definitively.

Average, median and mode statistics for the metallicity distributions are listed in Table 4, with numbers in parantheses based on $[\text{Fe}/\text{H}]$ values less than 0. The SMC fields generally come out more metal poor than the LMC fields, although the SMC HV11284 field appears to be nearly as metal-rich as the LMC HV12578 field. However, the uncertainty on the photometric zero-points translates to roughly 0.2 dex in $[\text{Fe}/\text{H}]$, so within the error limits the metallicities are consistent with the results from spectroscopic studies of F and G supergiants, $[\text{Fe}/\text{H}] = -0.3 \pm 0.2$ for the LMC and $[\text{Fe}/\text{H}] = -0.65 \pm 0.2$ for the SMC (Westerlund 1997). Our metallicities for the LMC fields are also consistent with those obtained by Dirsch et al. (2000) who quote $[\text{Fe}/\text{H}]$ values in the range -0.71 ± 0.23 to -0.52 ± 0.21 dex for young LMC clusters.

4.2. Investigating the effect of reddening

With the knowledge of reddenings obtained from B stars, it is possible to estimate how much of the apparent scatter in metallicity seen in Fig. 9 may actually be attributed to reddening variations.

In order to investigate how reddening variations affect the derived metallicity distributions, we carried out the following experiment: First, a set of $(b-y), m_1$ data pairs were generated, corresponding to one single metallicity (the canonical values were used for this experiment).

This was accomplished by using the list of observed $(b-y)$ indices and then generating the m_1 indices from the calibration equation. When plotted in the $(b-y), m_1$ diagram these points would then per definition fall along straight lines. Next, for each $(b-y), m_1$ data pair the reddening of a randomly selected B stars was added. The “metallicities” were then determined for these synthetic data using an *average* reddening, in the same way as for the real GK giants. This lead to the histograms drawn with dashed lines in Fig. 9.

The peaks of the simulated metallicity distributions are in quite good agreement with those of the actual observed distributions, at least to within the uncertainty arising from zero-point errors in the photometry. The scatter in the observed metallicity distributions remains somewhat larger than that of the simulated ones, and in particular, we note the presence of what might be interpreted as a metal-poor population, with metallicities extending down to $[\text{Fe}/\text{H}] \approx -2.0$. In order to quantify to what extent some of the scatter in the metallicity distributions may be intrinsic, we compared the observed and simulated distributions using an F-test (Press et al. 1992). For all the fields, the hypothesis that the variances of the two distributions are similar is rejected at a very high (> 99%) confidence level. This remains true even if the analysis is restricted to data with $[\text{Fe}/\text{H}] < 0$, except for the HV11284 field where no statistically significant difference is now found between the variances of the observed and simulated metallicity distributions.

It is instructive to consider what happens when one tries to compare e.g. the metallicity of cluster stars and the metallicity of surrounding field star populations: The cluster stars will all be located at the same depth in the LMC or SMC, so they will all be affected by the same amount of interstellar absorption. On the other hand, the field stars will be randomly distributed radially, and therefore their reddenings will vary accordingly. When metallicities are derived using Strömgen photometry one will indeed be able to confirm that the cluster stars all have the same metallicity, seemingly proving that the Strömgen photometry “works”, while the field stars will seem to occupy a wide range in metallicity. However, a significant amount of the scatter in the metallicities derived for the field stars may not be real, but is instead due to differences in the

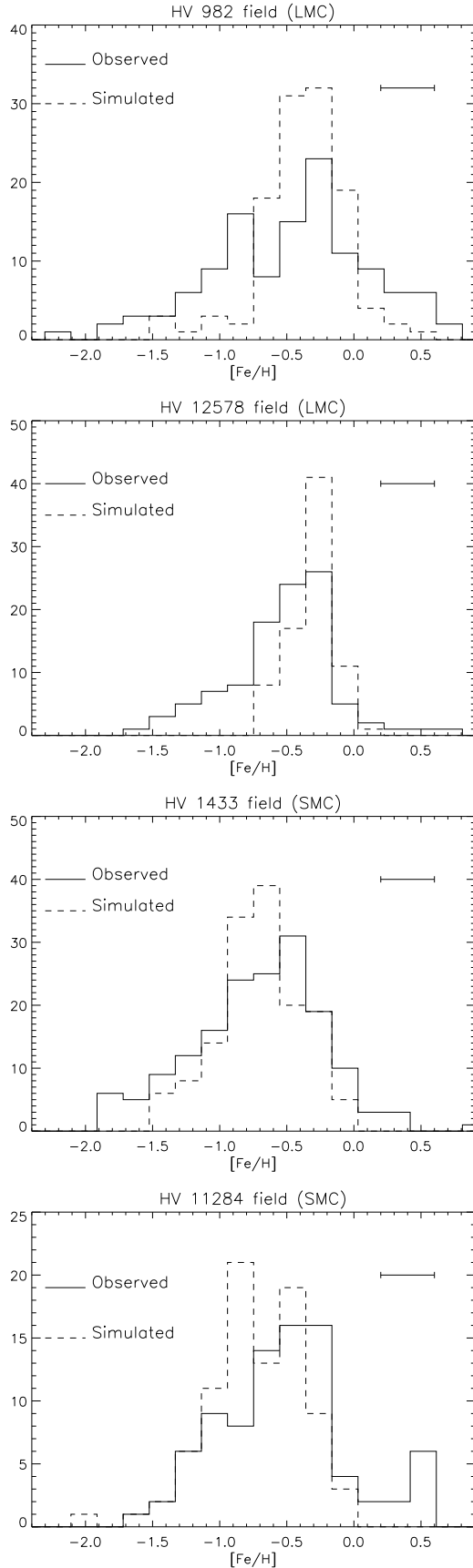


Fig. 9. Metallicities for the four fields; see text. The error bars refer to systematic errors due to zero-point errors in calibration of the photometry.

reddening from star to star. Any observed difference between the average field star metallicity and the cluster metallicity may be partly real, but will also depend on the amount of reddening internally in the SMC or LMC to which the cluster is subject.

For LMC/SMC clusters that are sufficiently young for early-type stars to be present it may be worthwhile to consider including u band observations in future Strömgren photometry so that reddenings can be determined. With the new generation of UV-sensitive CCD chips this will not be very costly in terms of observing time.

4.3. Ages

Independent age determinations for the metal-poor stars in our sample could provide insight into the age-metallicity relation for field stars in the Magellanic Clouds. Such a relation is relatively well established for *clusters* (e.g. van den Bergh 1991), but the situation for field stars is more uncertain due to the inherent difficulties in obtaining independent metallicities and ages. Here we will not attempt to derive age information for GK giants, but we note that Dirsch et al. (2000) attempted to determine an age-metallicity relation and the star formation history of both red giant field stars and clusters in their six LMC fields, using Strömgren vby photometry. They found evidence for an increase in the star formation rate ~ 3 Gyr ago, along with a rapid enrichment. However, the results remain uncertain because of possible CN anomalies in the LMC GK giants and the problems discussed in Sect. 4.2.

5. Summary and conclusions

Based on extensive Strömgren $uvby$ photometry we have investigated four $6' \times 4'5$ CCD fields, two in the LMC and two in the SMC. Because u -band observations were included it has been possible to study reddening variations on very small (~ 1 pc) scales.

From B stars we find that reddenings vary by several hundredths of a magnitude in $E(B-V)$ within a CCD field. The reddening variations are random rather than smooth, so unless the reddening for a particular object is directly measured it will be uncertain by at least 0.035 mag in $E(B-V)$ (HV 12578 field) and up to 0.10 mag (HV 11284 field). This translates directly into metallicity errors for red giants of 0.15 dex and 0.45 dex respectively, unless individual reddenings are available. We thus suggest that the u filter be included in LMC/SMC Strömgren photometry whenever possible. In particular, metallicity studies of young star clusters with a suitable number of B stars for reddening determinations would benefit strongly from the inclusion of u -band data.

Metallicities have been derived for GK giants. Within the ~ 0.2 dex uncertainties, the average metallicities are largely consistent with those derived from spectroscopic studies of F and G supergiants, about $[Fe/H] = -0.3$ for

the LMC and $[\text{Fe}/\text{H}] = -0.65$ for the SMC (Westerlund 1997), but we also see indications that a smaller number of more metal-poor stars with metallicities down to $[\text{Fe}/\text{H}] = -2.0$ are present in each of the fields. There are also hints of stars with higher metallicities, but this might be an effect of chemical peculiarities such as enhanced CNO abundances which are known to affect metallicities derived for red giants by means of Strömgren photometry in Galactic globular clusters (Dickens et al. 1979; Richter et al. 1999). Further follow-up spectroscopic studies are needed.

An unexpected byproduct of this study is the peculiar location of some early-type stars in the $[m_1], [c_1]$ diagram. Comparison with stellar models shows that this may be partly due to the lower-metallicity environments in the LMC and SMC, combined with the effect of random photometric errors. However, spectroscopy of some of the stars with peculiar indices would be highly desirable in order to check if the early-type stars in the LMC/SMC show other physical differences with respect to stars in the Solar neighbourhood.

Acknowledgements. ESO is gratefully acknowledged for granting a 2-months studentship to SSL in 1995, during which parts of the data reduction were carried out. This research was supported by the Danish Natural Science Research Council through research grants and through its Centre for Ground-Based Observational Astronomy. We thank the anonymous referee for useful suggestions and comments which helped improve the paper.

References

Bessell, M.S. 1991, A&A 242, L17
 Bond, H.E. 1980, ApJS 44, 517
 Clausen, J.V., Larsen, S.S., Garcia, J.M., Giménez, A., Storm, J. 1997, A&AS 122, 559
 Crawford, D.L. 1975, AJ 80, 955
 Crawford, D.L. 1978, AJ 83, 48
 Crawford, D.L., Glaspey, J.W., Perry, C.L. 1970, AJ 75, 822
 de Boer, K.S., Azzopardi, M., Baschek, B., Dennefeld, M., Israel, F.P., Molaro, P., Seggewiss, W., Spite, F., Westerlund, B.E. 1989, The ESO Messenger 57, 27
 Dickens, R.K., Bell, R.A., Gustafsson, B. 1979, ApJ 232, 428
 Dirsch, B., Richtler, T., Gieren, W.P., Hilker, M. 2000, A&A 360, 133
 Girardi, L., Bressan, A., Bertelli G., Chiosi C. 2000, A&A Suppl. Ser. 141, 371
 Grebel, E.K., Richtler, T. 1992, A&A 253, 359 (GR92)
 Grieve, G.R., Madore, B.F. 1986, ApJS 62, 427
 Harris, J., Zaritsky, D., Thompson, I., 1997, AJ 114, 1933
 Hilker, M. 2000, A&A, 355, 994
 Hilker, M., Richtler, T., Gieren, W. 1995, A&A 294, 241 (HRG95)
 Hill, V. 1999, A&A 345, 430
 Knude, J. 1993, A&AS 99, 499
 Kurucz, R., 1979, ApJS 40, 1
 Kurucz, R., 1992, IAU Symp 149, 225
 Larsen, S.S. 1996, Master Thesis, Astronomical Observatory, Copenhagen University

Oestreicher, M.O., Goehermann, J., Schmidt-Kaler, T. 1995, A&AS 112, 495
 Oestreicher, M.O., Schmidt-Kaler, Th. 1996, A&AS 117, 303
 Olsen, E.H. 1979, A&AS 37, 367
 Olsen, K.A.G. 1999, AJ 117, 2244
 Olszewski, E. W., Schommer, R. A., Suntzeff, N. B., Harris, H. C. 1991, AJ 101, 515
 Press W.H., Teukolsky S.A., Vetterling W.T., Flannery B.P., 1992, Numerical Recipes in C/Fortran, second ed. Cambridge University Press
 Richter, P., Hilker, M., Richtler, T. 1999, A&A, 350, 476
 Romaniello, M., Salaris, M., Cassini, S., Panagia, N. 2000, ApJ 530, 738
 Savage, B.D., Mathis, J.S. 1979, ARA&A 17, 73
 Schechter, P.L., Mateo, M., Saha, A. 1993, PASP 105, 1342
 Schlegel, D.J., Finkbeiner, D.P., Davis, M., 1998, Ap J 500, 525
 Spite, M., Spite, F. 1987, ESO Messenger, June 1987, 48, 37
 Stetson, P. 1987, PASP 99, 191
 Strömgren, B. 1966, ARA&A 4, 433
 van den Bergh, S. 1991, ApJ 369, 1
 Westerlund, B.E. 1990, A&AR 2, 29
 Westerlund B.E. 1997, *The Magellanic Clouds*, Cambridge University Press
 Zaritsky, D. 1999, AJ 118, 2824